

## Decoupling the Doppler Ambiguity Interval from the Maximum Operational Range and Range-Resolution in FMCW Radars

Neemat, Sharef; Krasnov, Oleg; van der Zwan, Fred; Yarovoy, Alexander

**DOI**

[10.1109/JSEN.2020.2972152](https://doi.org/10.1109/JSEN.2020.2972152)

**Publication date**

2020

**Document Version**

Final published version

**Published in**

IEEE Sensors Journal

**Citation (APA)**

Neemat, S., Krasnov, O., van der Zwan, F., & Yarovoy, A. (2020). Decoupling the Doppler Ambiguity Interval from the Maximum Operational Range and Range-Resolution in FMCW Radars. *IEEE Sensors Journal*, 20(11), 5992-6003. Article 8988231. <https://doi.org/10.1109/JSEN.2020.2972152>

**Important note**

To cite this publication, please use the final published version (if applicable).  
Please check the document version above.

**Copyright**

Other than for strictly personal use, it is not permitted to download, forward or distribute the text or part of it, without the consent of the author(s) and/or copyright holder(s), unless the work is under an open content license such as Creative Commons.

**Takedown policy**

Please contact us and provide details if you believe this document breaches copyrights.  
We will remove access to the work immediately and investigate your claim.

***Green Open Access added to TU Delft Institutional Repository***

***'You share, we take care!' - Taverne project***

**<https://www.openaccess.nl/en/you-share-we-take-care>**

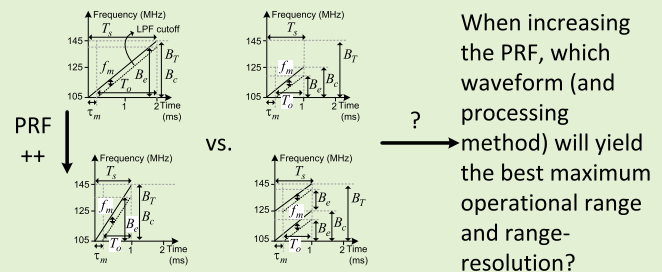
Otherwise as indicated in the copyright section: the publisher is the copyright holder of this work and the author uses the Dutch legislation to make this work public.

# Decoupling the Doppler Ambiguity Interval From the Maximum Operational Range and Range-Resolution in FMCW Radars

Sharef Neemat<sup>1</sup>, Oleg Krasnov<sup>1</sup>, Fred van der Zwan, and Alexander Yarovoy, *Fellow, IEEE*

**Abstract**—Classical saw-tooth Frequency Modulated Continuous Wave (FMCW) radars experience a coupling between the maximum unambiguous Doppler-velocity interval, maximum operational range, range-resolution and processing gain. Operationally, a trade-off is often necessarily made between these parameters. In this paper, we propose a waveform and a processing method that decouples the aforementioned parameter dependencies at the price of using multiple receiver channels within the radar. The proposed method exploits the fact that beat-frequency signals have the same baseband frequency, even if the transmitted and received chirps occupy different radio frequency bands, and have different center-frequencies. We concatenate those baseband signals in the time-frequency domain to restore the range-resolution and processing gain. An overview of FMCW parameters trade-off for related waveforms and a feasibility and limitations analysis of implementing the proposed processing method are presented. The method is verified by simulations and experiments with an FMCW radar for stable, moving and extended-moving targets. We additionally have highlighted its non-idealities in the simulations and experiments. We found that the proposed method indeed alleviates the trade-off between FMCW operational parameters and allows the extension of the Doppler ambiguity interval without compromising on those parameters.

**Index Terms**—Beat-Frequency, frequency-modulated continuous-wave (FMCW), maximum range, range-resolution, unambiguous doppler-velocity.



## I. INTRODUCTION

**F**REQUENCY Modulated Continuous Wave (FMCW) radars [1], [2] operating with chirp-sequence saw-tooth waveforms in deramping (stretch-processing) mode are widely used for numerous applications. Such as weather observation, automotive sensing and navigation [3], and biomedical [4]. The deramping processing concept is based on the mixing of the transmitted signal with the received echoes, resulting in baseband signals known as beat-signals.

After deramping – for a single point-target, the time delay between the probing signal transmission and the scattered signal reception will result in a single-tone signal, known as a

beat-frequency, whose frequency is proportional to that target's range. Range is therefore defined by frequency. To elaborate, this single-tone beat-signal for that point-target is observed during a certain time interval within the radar's sweep time. Classical signal compression is then done by converting this single-tone signal to the spectral domain. As a result, the point-target is represented as a sinc-function-shaped spectral line which has a bandwidth that is inversely proportional to the duration of the signal observation time interval. The conversion of this compressed signal from the spectral domain to the range domain (to produce a range-profile) is done by rescaling the spectrum grid to a range grid using a scaling equation. As a result, the sinc-function-shaped spectral line – related to that point-target – is converted into what can be called a point target response function (analogous to the impulse response function in pulse-compression radar). In classical FMCW processing, the width of this response function after scaling is inversely proportional to the transmitted bandwidth during the observation time interval. This width represents the actual radar range resolution, which is directly proportional to the target's range localization accuracy. A radar's range-resolution

Manuscript received January 22, 2020; revised February 4, 2020; accepted February 4, 2020. Date of publication February 10, 2020; date of current version May 5, 2020. The work of Sharef Neemat was supported by the KACST Scientific Institution. The associate editor coordinating the review of this article and approving it for publication was Dr. Marco J. Da Silva. (Corresponding author: Sharef Neemat.)

The authors are with the Group of Microwave Sensing, Signals and Systems, Delft University of Technology, 2628CD Delft, The Netherlands (e-mail: s.a.m.neemat@tudelft.nl; o.a.krasnov@tudelft.nl; w.f.vanderzwan@tudelft.nl; a.yarovoy@tudelft.nl).

Digital Object Identifier 10.1109/JSEN.2020.2972152

is a criteria by which the radar's ability to separate targets that are close in range is evaluated. The radar's chirp-rate defines the ratio between the transmitted bandwidth and the sweep time (PRI). The radar's maximum operational range is defined by its maximum beat-frequency, which is typically set by a Low Pass Filter (LPF) placed subsequent to the mixing of the transmitted and received signals. Targets' velocities are typically calculated from Doppler frequency estimation across multiple targets' returns from multiple sweeps in a Coherent Processing Interval (CPI). The radar's sweep repetition frequency (PRF) is therefore the Doppler sampling frequency, and in consequence defines the radar's maximum unambiguous velocity. The FT is widely used for the estimation of target ranges and velocities, for its compatibility with most processing architectures, linearity and predictable latency.

The problem this paper offers a solution for is the coupling of the radar's Doppler-velocity ambiguity interval – as defined by the PRF, with its range-resolution, processing gain, and its maximum operational range. This is in the sense that if there is an operational requirement for the observation of fast(er) moving targets, conventional FMCW radar requires the utilization of a higher PRF, which in turn reduces the range-resolution due to the reduced transmitted bandwidth because of the reduced observation time. But, if the transmitted bandwidth is to be maintained as it was before increasing the PRF – by increasing the chirp-rate, which is not always possible for legacy systems – the maximum operational range will be reduced due to the fixed LPF cutoff frequency. The developed solution shall not require any detection or a-priori information about the observed scene, shall be applicable to very-extended targets like rain/clouds, and shall only use the FT – as opposed to iterative frequency estimation techniques.

Previous work on the topic of decoupling FMCW radar operational parameters is here reviewed. The method in [5] doubles the range-resolution refinement without transmitting extra bandwidth, but is restricted to the chirp center-frequency being an integer multiple of the total transmitted bandwidth, and without improvement to the Doppler ambiguity interval. Under-sampling or antenna-spacing schemes are ways to increase range-resolution, but still suffer from Doppler ambiguities [6], [7]. The work in [8] utilizes a Bandwidth Extrapolation (BE) method which uses an Auto Regressive (AR) model to interpolate beat-signals to connect multiple RF sub-band returns in fast-time to improve the resolution. The technique is not suitable for systems with an LPF cutoff of a few MHz – in addition to a usually unknown number of observed targets – yielding a fast-time signal which would require an AR filter order in thousands to interpolate, which is very difficult to realize and implement in a practical system. The improvement from BE methods is also typically limited to small durations of a sweep, and it would not be realistic if there is a desire to increase the PRF by a factor of 2, since that would mean that half of the original signal would have to be interpolated. The method in [9] is also a BE technique for matched-filter processing and is not applicable to deramping systems. An iterative frequency estimation method for synthesizing a wideband waveform from discontinuous

bands to improve resolution is presented in [10]. The method is free from restriction related to the maximum center-frequency separation between utilized sub-bands, but does not rely on the FT, making its latency unpredictable since it relies on algorithm convergence. An interesting approach which unbinds the Doppler ambiguity interval from the PRF is presented in [11], but requires the usage of time-shifted opposite-slope chirps, and is iterative along target-peaks, making it unsuitable for extended meteorological targets like rain. The method in [12] decouples the maximum range from the Doppler velocity interval by processing received signals in overlapping sections of two sweeps (using a synthetically stored chirp). That is at the cost of higher computational complexity and being limited to only using two chirps. For the high computational price of using neural networks, the work in [13] introduces a methods to decouple range resolution from the PRF.

The solution proposed in this paper is the multiplexing of multiple chirps within one sweep, and a processing method that decouples the aforementioned parameter dependencies at the price of using multiple receiver channels within the radar. The processing method will exploit the fact that beat-frequency signals have the same baseband frequency – even if the transmitted and received chirps occupy different RF bands, and have different center-frequencies (with restrictions further discussed in the paper). The fusion of those – same frequency – baseband signals will be done in the time-frequency domain using phase shift operations. The solution will enable the radar to continuously operate at a high PRF, liberating it from post range-Doppler resolution improvement techniques which might suffer from Doppler frequency spectrum folding due to the ambiguities related to a low PRF.

The novelty of this work and difference from previous techniques is highlighted in:

- 1) The first ever processing method for the coherent integration of frequency multiplexed chirps within one sweep/PRI – for deramping FMCW radar in the time-frequency domain, which allows the decoupling of the Doppler ambiguity interval from the maximum range, processing gain and range-resolution.
- 2) The method constructs a single fast-time slow-time matrix – with an extended Doppler ambiguity interval, restored range resolution and restored CPI processing gain – in one go.
- 3) The method does not use iterative algorithms with unpredictable latencies, nor requires any detection or a-priori information about the observed scene, and is applicable to very-extended targets like rain/clouds.

The rest of this paper is organized as follows: Section II presents related theoretical aspects. Section III presents the method for multiple sub-bands sweeps concatenation in the time-frequency domain. Section IV discusses the implementation feasibility of the proposed method. Section V presents simulations, experimental verification with real radar data and discusses the findings. Conclusions and final remarks are covered in Section VI.

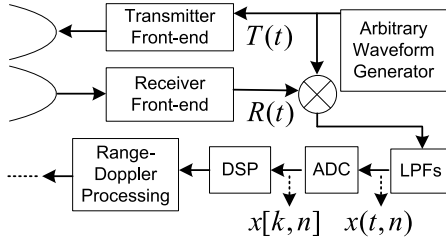


Fig. 1. Simplified deramping FMCW radar block diagram. The transmitted and received signals are mixed to produce beat-frequency signals, filtered and digitized for further processing.

## II. THEORY

### A. Related FMCW Radar Background

An FMCW radar [1] like the one depicted in Fig. 1 transmits a saw-tooth signal which can be expressed as:

$$T(t) = A_t \text{rec}\left(\frac{t}{T_s}\right) \cos\left[2\pi\left(f_c t + \frac{1}{2}\alpha t^2\right)\right] \quad (1)$$

for  $-T_s/2 < t < T_s/2$ , where  $T_s$  is the sweep time/Pulse Repetition Interval (PRI).  $A_t$  is the amplitude,  $f_c$  the carrier center frequency, and the chirp-rate  $\alpha$  is:

$$\alpha = B_c/T_s \quad (2)$$

where  $B_c$  is the transmitted chirp bandwidth. The chirp-rate preceding sign determines if it is an up-chirp or a down-chirp. The radar receives an echo signal from a target after a time delay  $\tau$ , which can be expressed as:

$$R(t) = A_r \text{rec}\left(\frac{t}{T_o}\right) \cos\left[2\pi\left(f_c(t - \tau) + \frac{1}{2}\alpha(t - \tau)^2\right)\right] \quad (3)$$

for  $-T_o/2 < t < T_o/2$ , where  $A_r$  is the received amplitude. The observation time  $T_o$  (ADCS sampling interval) is related to the sweep time as:

$$T_o = T_s - \tau_m \quad (4)$$

where  $\tau_m$  the maximum system delay corresponding to the desired radar maximum range. A target's delay is therefore related to its range as:

$$\tau = 2(R_0 + vt)/c \quad (5)$$

where  $R_0$  is its initial range and  $v$  its velocity.

In deramp (de-chirp) processing, the transmitted signal is mixed with the received one to produce – after proper filtration – what is known as a beat signal. This signal is in baseband and can be expressed – after simplification and discarding of usual negligible terms in a narrow-band system with no accelerating targets – for the  $n^{\text{th}}$  sweep in a CPI, following [14] and [15], as:

$$x(t, n) = A_b \cos\left[2\pi\left(\frac{2\alpha R_0}{c}t + \frac{2f_c v}{c}t + \frac{2v B_c n}{c}t + \frac{2f_c v n}{c}T_s\right)\right] \quad (6)$$

where  $t$  is fast-time within the sweep and  $A_b$  the beat signal amplitude. Estimating the frequency term  $\frac{2\alpha R_0}{c}$  provides the target range. The second and third terms are the usual

FMCW range-Doppler coupling terms. The target's velocity  $v$  is estimated from the phase evolution in the phase term  $(\frac{2f_c v n}{c}T_s)$  over multiple sweeps in a CPI ( $nT_s$ ), hence the 2-D FT typically performed on beat-signals from multiple sweeps in a CPI to estimate range and velocity.

It then follows that the estimated frequency term – known as the beat-frequency – is related to the target's range, and that the maximum operational range  $R_m$  is related to a maximum beat-frequency  $f_m$  as:

$$f_b = \frac{2\alpha R_0}{c}, \quad f_m = \frac{2\alpha R_m}{c}. \quad (7)$$

The target range is then:

$$R_0 = \frac{c}{2\alpha} f_b. \quad (8)$$

These relations can also be derived from the triangle's geometry as depicted in Table I waveform (W.a). For the cases in the table, we can observe the  $(\tau_m, f_m)$  relation from the drawings, in the sense that the LPF implementing the  $f_m$  cutoff-frequency defines the maximum range  $R_m$  in de facto. The effective bandwidth is related to the transmitted on by:

$$B_e = \frac{B_T T_o}{T_s}, \quad (9)$$

which also expresses the degradation in the transmitted bandwidth due to the reduced observation time ( $T_o < T_s$ ). The range-resolution is therefore:

$$\Delta R = \frac{c}{2B_e}. \quad (10)$$

The unambiguous Doppler-velocity interval  $v_u$  is defined by the PRF as:

$$v_u = \pm \frac{\lambda \text{PRF}}{4} \quad (11)$$

where  $\lambda$  is the wavelength. The sweep compression gain (also known as the BT time-bandwidth product) [16] is:

$$G_r = B_e T_o. \quad (12)$$

The total processing gain in a CPI is the BT product multiplied by the number of sweeps in the CPI ( $N_{\text{CPI}}$ ):

$$G_{\text{CPI}} = G_r N_{\text{CPI}}. \quad (13)$$

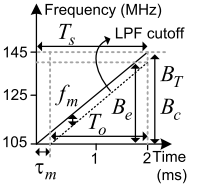
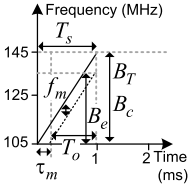
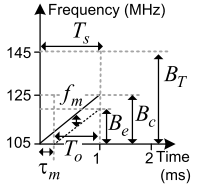
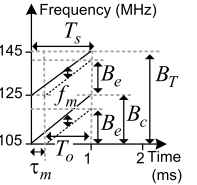
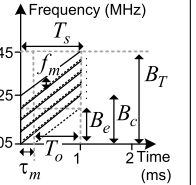
Note that waveforms presented in Table I will be further used in the paper for discussions, simulations and experiments, and that the frequency values are in intermediate frequency (IF) before up-conversion to RF.

### B. Operational Parameters Trade-Offs

The waveform in the first column (W.a) of Table I is to be taken as the reference case for the following trade-off analysis. If there is a desire to increase  $v_u$  by a factor of 2 for the unambiguous observation of fast(er) moving targets, the PRF needs to be increased by a factor of 2. The options for this – in standard processing – are presented in cases (W.b) and (W.c), where the number of sweeps in a CPI  $N_{\text{CPI}}$  is increased by a factor of 2 in an attempt to recover any possible processing gain loss. For waveform (W.b), changing the chirp-rate to cover the entire available bandwidth might not be possible

TABLE I

WORKED-OUT TRADE-OFFS FOR WAVEFORMS DISCUSSED IN THE THEORY SECTION II, THE SIMULATIONS AND THE EXPERIMENTS IN SECTION V. WAVEFORMS W.A, W.B AND W.C REPRESENT CLASSICAL OPERATION, WHEREAS W.D AND W.E THE PROPOSED PROCESSING METHOD

										
Waveform	W.a		W.b		W.c		W.d		W.e	
Description	Standard reference chirp		Double the PRF and increase sweep-rate to cover entire available bandwidth		Double the PRF but keep sweep-rate as in W.a		Double the PRF and keep sweep rate as in W.a, but use two chirps		Double the PRF and keep sweep rate as in W.a, but use five chirps	
Chirps per sweep/PRI $M$	1		1		1		2		5	
Sweeps in CPI $N$	32		64		64		64		64	
Max. round-trip time $\tau_{\max}$ (5) ( $\mu s$ )	100		100		100		100		100	
Max. beat-freq. $f_m$ (LPF) (7) (MHz)	2	15	2	7.5	2	15	2	15	2	15
Max. range $R_m$ (7) (Km)										
Sweep time $T_s$ (1) (ms)	2	0.5	1	1	1	1	1	1	1	1
PRF (1) (KHz)										
Max. Unambiguous Doppler Velocity (11) (m/s)	11.3		22.6		22.6		22.6		22.6	
Observation time (4) (ms)	1.9		0.9		0.9		0.9		0.9	
Total available bandwidth $B_T$ (1) (MHz)	40		40		40		40		40	
Transmitted chirp bandwidth $B_c$ (2) (MHz)	40		40		20		20 per chirp		20 per chirp	
Effective bandwidth $B_e$ (9) (MHz)	38		36		18		18 per chirp		18 per chirp	
Chirp-rate $\alpha$ (2) (GHz/s)	20		80		20		20		20	
Range resolution $\Delta R$ (10) (m)	3.9		4.1		8.3		4.1		4.1	
CPI processing gain $G_{CPI}$ (13)	2310400		2073600		1036800		2073600		5184000	

for legacy systems, and will result in a maximum range  $R_m$  loss by a factor of 2 for the same LPF cutoff frequency. The benefits on the other hand would be that the range-resolution  $\Delta R$  and the processing gain  $G_{CPI}$  will not degrade by a factor of 2. For waveform (W.c),  $R_m$  is maintained in reference to (W.a), but  $\Delta R$  and  $G_{CPI}$  are worst by almost a factor of 2 – due to not using the entire available bandwidth – even for the same  $N_{CPI}$ . The improvements when using waveforms (W.d) and (W.e) will be covered in the next subsection.

### C. Operational Parameters Decoupling

The method described in Section III exploits the fact that beat-signals have the same baseband frequency, even if the

transmitted and received chirps occupy different RF bands. The method will show how these beat-signals can be chained together for further usage. This will mean that the more chirps the radar can transmit and receive, the more beat-frequency samples are available for usage. The feasibility and limitations of this will be covered in Section IV. These extra beat-frequency samples will mean that we can increase the PRF, and therefore increase the unambiguous Doppler-velocity interval (while maintaining the same chirp-rate and maximum range  $R_m$ ). All that without compromising on the range resolution and CPI processing gain.

We demonstrated in previous work [17] that – for a single-receiver-channel deramping FMCW radar – the target response function width can be improved by concatenating beat-signals



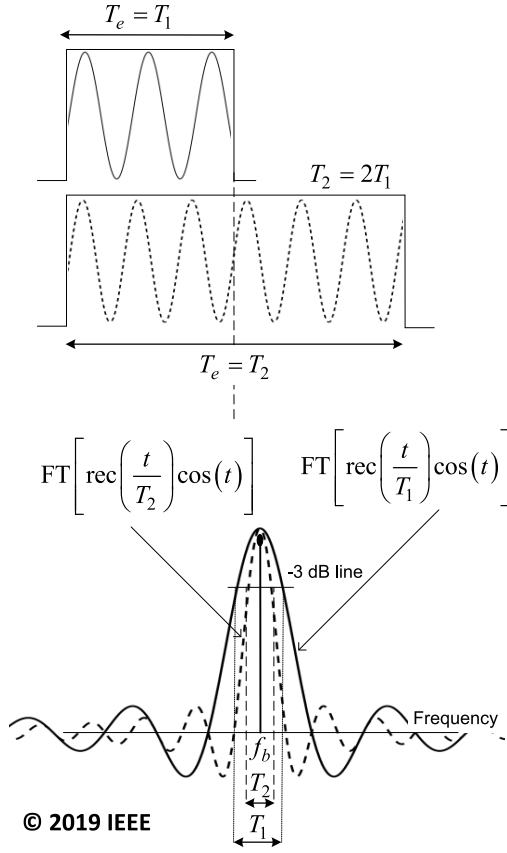


Fig. 2. Simplified *sinc* function spectral bandwidth illustration for signals with different durations/number of samples. When coherently concatenating two – or more – chirps, the *sinc* function 3 dB width will reduce [17].

from multiple sweeps in a CPI. In this paper we demonstrate the improvement by concatenating two or more chirps from the same sweep/PRI using multiple receivers, which in essence decouples the CPI processing gain and range-resolution from the Doppler ambiguity interval, at the price of using those multiple deramping receivers.

The signal processing concept behind the target response function width improvement is depicted in Fig. 2, where the frequency spectrum width is defined by the 3 dB width of the *sinc* function centered around  $f_b$  [18], [19]. This means that the width is inversely proportional to the integration time:

$$\Delta f = 1/T_e. \quad (14)$$

In the figure, the additional samples added to the signal were expressed in terms of time since it was indeed a concatenation along the time axis from two or more sweeps in [17], which in essence increased the integration time.

If the chirp sampling frequency is  $f_s$ , we now propose the improvement to be expressed in number of samples instead of time ( $\Delta f = f_s/(KM)$ ), since the extra samples come from the same sweep/PRI (as seen in waveforms (W.d) and (W.e) in Table I).

Assuming the time domain sample index in a chirp is  $k$ , where  $k = 1, \dots, K$ , and  $K = f_s T_o$ . The improvement in the

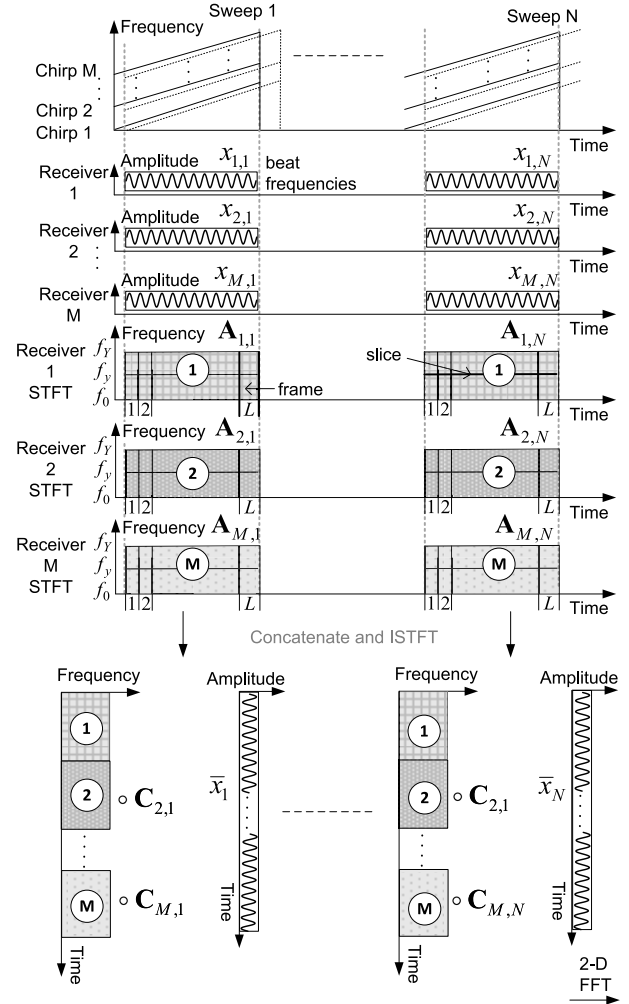


Fig. 3. Graphical illustration of the proposed processing technique described in Section III. STFT data from multiple chirps in the same sweep – handled by multiple receivers – are concatenated in the STFT domain to produce longer coherent signals for further range-Doppler processing. Note that ‘slice’ indicates a frequency-slice ( $f_y$  for example), and ‘frame’ indicates a time-frame ( $L$  for example). The frequency-time and amplitude-time representations at the bottom of the figure are a depiction of the resultant concatenated time frequency matrices and the resultant extended beat frequency signal respectively.

target response function width can thus be expressed as:

$$\Delta f_M = \frac{f_s}{kM} \quad (15)$$

where  $M$  is the number of frequency chirps multiplexed in a sweep, and is therefore also the number of receivers in the system. This is shown in the drawings and calculations of waveforms (W.d) and (W.e) in Table I. It then follows that the improvement in the processing gain in (12) after concatenating  $M$  sweeps can now be expressed as:

$$\bar{G}_r = B_e T_o M. \quad (16)$$

### III. METHOD: SUB-BANDS SWEEPS CONCATENATION

Chirps from different sub-bands in a sweep are coherently concatenated in the time-frequency domain using phase-shift operations, as depicted in Fig. 3. As the steps will show,

working in the time-frequency domain allows for better phase evolution estimations, and opens the possibility to extrapolate frequency slices to compensate for the dead-time region between sweeps as in [17]. The steps are:

- 1) Store the deramped time-domain beat-frequency signal output from each receiver in the system. These signals can be expressed as  $x_{m,n}[k]$ . The receiver number is  $m$ , and  $1 \leq m \leq M$ , where  $M$  is the number of receivers in the system. The sweep number in the CPI is  $n$ , and  $1 \leq n \leq N$ , where  $N$  is the total number of sweeps in that CPI.
- 2) Take sweeps from all receivers to the time-frequency domain by applying an STFT, where a sweep can be expressed in matrix form as

$$\mathbf{A}_{m,n}[l, y] = \left[ \sum_{q=-\frac{W}{2}}^{\frac{W}{2}-1} w[q] x_{m,n}[q - l\Delta h] e^{-i2\pi qy/W} \right]_{Y \times L} \quad (17)$$

with  $Y$  rows and  $L$  columns, where  $l$  is the STFT frame index,  $l = 1, \dots, L$ , and  $L = 1 + \lfloor (k - W)/\Delta h \rfloor$ . The analysis window length is  $W$ . The STFT hop size is  $\Delta h$ , and  $\lfloor \cdot \rfloor$  denotes the floor operation. The frequency-slice index in the STFT frequency grid is  $y$ , where  $y = 0, \dots, Y$ , and  $Y$  is the maximum beat-frequency index. The analysis window (for instance, Hamming) is  $w$ . The selection of the STFT window and hop sizes should be application dependent, and their selection trade-offs have been studied in [20].

- 3) Form concatenated slices in the STFT domain from all receivers as:

$$\mathbf{P}_n = [\mathbf{A}_{1,n} \ \mathbf{A}_{2,n} \circ \mathbf{C}_{2,n} \ \dots \ \mathbf{A}_{m,n} \circ \mathbf{C}_{m,n}]_{Y \times (M \cdot L)} \quad (18)$$

where ‘ $\circ$ ’ denotes the Hadamard product. The phase matching term  $\mathbf{C}$  has  $L$  identical columns, and is defined as

$$\mathbf{C}_{m,n} = \begin{bmatrix} e^{i\Delta\varphi_m(f_0)} & \dots & e^{i\Delta\varphi_m(f_0)} \\ \vdots & \vdots & \vdots \\ e^{i\Delta\varphi_m(f_Y)} & \dots & e^{i\Delta\varphi_m(f_Y)} \end{bmatrix}_{Y \times L} \quad (19)$$

where

$$\Delta\varphi_m(f_y) = (\varphi_{m-1,L}(f_y) - \varphi_{m,1}(f_y)) + (2\pi f_y t_h). \quad (20)$$

The frequency value at a frequency-slice index is  $f_y$ , and the hop time  $t_h = \Delta h/f_s$ . Since this is done in the time-frequency domain, the term  $2\pi f_y t_h$  in (20) can alternatively be calculated by taking the mean of the differences between the – unwrapped – phase values for every frequency slice. Note that the phase matching operations insure phase continuity for each frequency slice when performing an Inverse STFT (ISTFT) in the next step.

- 4) Form the new time-domain concatenated beat-frequency sweep by applying an ISTFT as

$$\tilde{x}_n = \text{ISTFT}(\mathbf{P}_n). \quad (21)$$

#### IV. IMPLEMENTATION FEASIBILITY AND LIMITATIONS

The following subsections analyze the feasibility of operating a multi receiver channel radar with waveforms such as (W.d) and (W.e) in Table I.

##### A. Receiver Channels Calibration

As will be demonstrated in the experiments section, multiple receivers used for the collection of beat-signals need to be calibrated in amplitude and phase. Mismatches in a fast-time slow-time matrix before – Doppler processing – can be thought of as the superimposition of a second sin wave on top of an original one that is sampled for Doppler processing. That then causes grating lobe in the opposite Doppler-velocity spectrum, which may be interpreted as ghost targets.

##### B. Maximum Number of Chirps in a Sweep/PRI

Assuming the radar receiver channels implement a deramping Single-Sideband (SSB) I/Q architecture with the ability to reject negative frequencies, the maximum number of chirps which can be stacked in a single sweep/PRI – inferred from triangle geometry in the depiction of (W.e) in Table I – is:

$$M_{\max} = \left\lfloor \frac{B_T - B_c}{f_m} \right\rfloor + 1 \quad (22)$$

where the SSB’s LPF cutoff-frequency defines  $f_m$  as in (7). It is worth noting that this assumes a sharp filter cutoff with no guard-band, where in reality, such a filter is difficult to realize. Note that the SSB receiver is what allows each radar receiver to reject interfering echos from other receivers. This is in the sense that a positive frequency echo for one chirp will appear as a negative echo for another chirp, and with the SSB I/Q implementation, these interfering echos can easily be rejected.

##### C. Maximum Chirps’ Center-Frequency Difference

For the same observed target with two different center-frequency  $f_c$  chirps within the same sweep, the beat-frequency follow the form as in (6). The only difference in the calculated frequency terms in the beat frequency  $f_b$  from (6) is then:

$$\Delta f_b = \frac{2v(f_{c2} - f_{c1})}{c}. \quad (23)$$

Since the method described in Section III concatenates beat-frequency slices in the STFT domain, the target will appear in the same STFT slice grid, as long as the difference is smaller than the STFT frequency grid resolution as:  $\Delta f_b < \Delta f_{STFT}$ , where  $\Delta f_{STFT} = f_s/W$ , and  $W$  is the STFT window length as in (17).

##### D. Limitations

The limitations for the proposed method are SNR, system non-linearities – in the transmitter and receiver – and accumulating concatenation errors. Low SNR will result in poor phase estimations and concatenation errors. Because of non-linearities, even a point-target will have a certain 3 dB spectral width dictated by the radar’s non-linearities [14] as:  $\Delta f_{\text{target}} =$



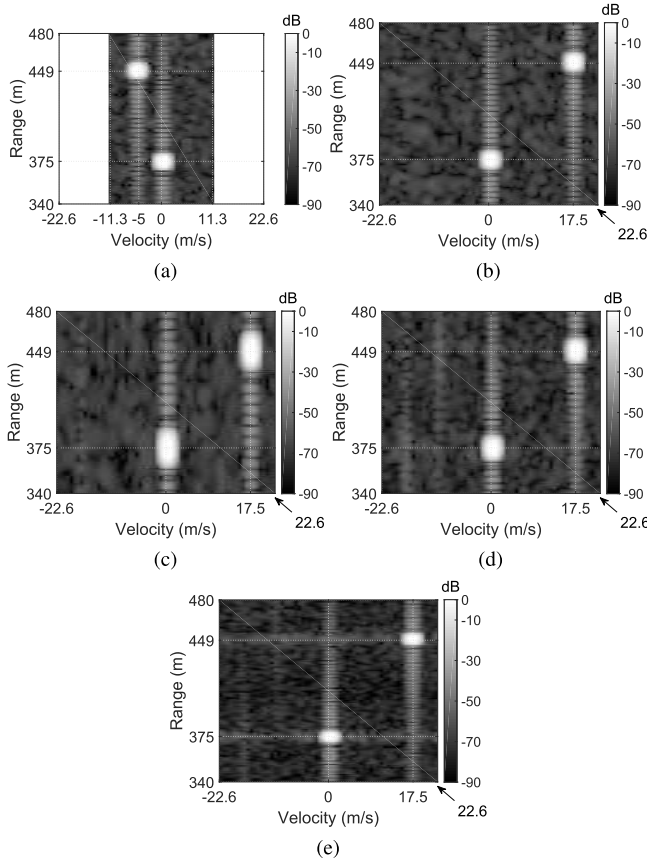


Fig. 4. Simulation results for the different waveforms in Table I. Two targets are simulated, G1 and G2, with the parameters in Table II, and an SNR of 20 dB. The extension of the unambiguous Doppler-velocity interval allows for target G2's velocity of 17.5 m/s to be unambiguously estimated for waveforms (W.b), (W.c), (W.d) and (W.e), as shown in (b), (c), (d) and (e) respectively. Targets' response function width when using (W.a) – as seen in (a) – is almost restored for waveforms (W.d), and improved for (W.e) as expected.

$\Delta f_{\text{target}} + (\chi/100)\Delta f_{\text{target}}$ , where  $\chi$  is the non-linearity in percentage. Any concatenation errors will also result in grating-lobes and spectral width widening. The method is also not suitable for targets which have a substantially high acceleration, to the point that a target's beat-frequency changes *within* one sweep, with a value greater than that of the STFT frequency grid resolution. An example is missile tracking applications.

## V. SIMULATIONS AND EXPERIMENTAL VERIFICATION

### A. Simulations

A simulation of the different waveform cases in Table I is presented in this section with the parameters in Table II for two point-targets. White Gaussian noise is added and targets are simulated for different SNR values (20, 13, 0 and –40 dB). The SNR values are for the beat frequency signal for a single receiver before any processing. Note that the chirp frequency values in Table I are in Intermediate Frequency (IF) before up-conversion to S-band RF, where the 125 MHz is up-converted to an  $f_c$  equal to 3.315 GHz. This  $f_c$  is selected to match that of the experimental radar in the next subsection. For the 20 dB SNR case, the range-Doppler results

TABLE II  
SIMULATION AND PROCESSING PARAMETERS

Simulation Parameters			
Target number	Range (m)	Velocity (m/s)	Wavelength $\lambda$ (m)
G1	375	0	0.0905
G2	449	17.5	
STFT Processing Parameters			
Window length $W$	7168		
Hop size $\Delta h$	8		

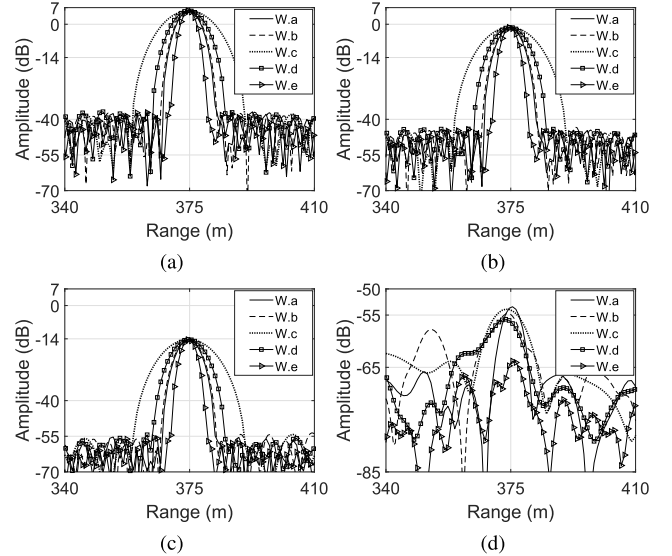


Fig. 5. Simulation results for the different waveforms in Table I. A range cut through zero-Doppler shows the response function width achieved by all waveforms for target G2. Sub-figures (a), (b), (c) and (d) are for simulations with SNR values 20, 13, 0 and –40 dB respectively. In (d), the SNR is –40 dB, and the proposed method suffers from concatenation errors as discussed in the limitations subsection.

for (W.a), (W.b), (W.c), (W.d) and (W.e) are presented in Fig. 4(a), (b), (c), (d) and (e) respectively.

The stable target G1 remains at zero-Doppler for all waveforms as expected. Target G2 has a velocity of 17.5 m/s, but  $v_u$  for (W.a) is 11.3 m/s, causing the target to be ambiguously folded to around –5 m/s. For the remaining cases, the velocity is unambiguously estimated after increasing the PRF to 1 kHz. The target response function width loss for both targets is apparent for case (W.c), and its maintenance in relation to (W.a) can be seen in cases (W.b), and to a large extent in (W.d). A significant target response function width improvement can be observed for case (W.e) as expected. Range-cuts through the range-Doppler maps for target G2 are presented in Fig. 5(a), (b), (c) and (d) for SNR values of 20, 13, 0 and –40 dB respectively, where the effects on the target response function width for all cases is observed. In Fig. 5(d) the SNR is dropped to –40 dB, and the proposed method suffers from concatenation errors as discussed in the limitations subsection.

### B. Experimental Setup

The method is experimentally demonstrated using the Delft University of Technology (TU Delft) PARSAX FMCW radar [21] mounted on a building roof on campus, as shown in

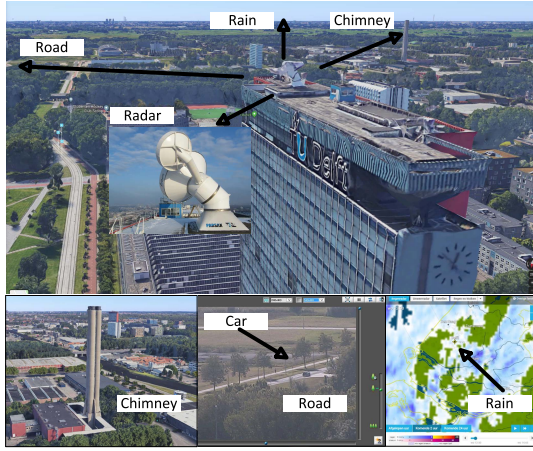


Fig. 6. The experimental PARSAX radar mounted on the roof, and targets used for experiments in Section V.

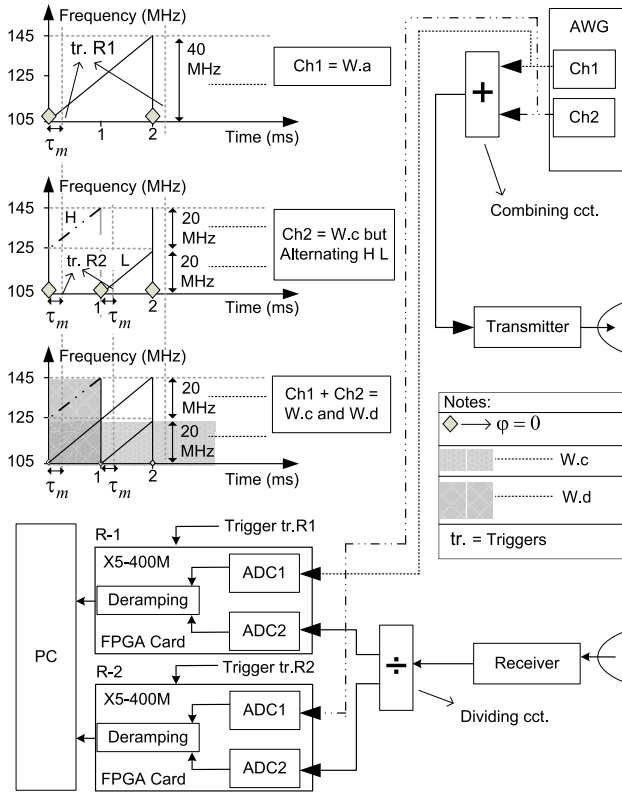


Fig. 7. Simplified radar block diagram and experimental verification setup related to the discussion in Section V-B.

Fig. 6. The experiment was setup to always have a reference waveform to compare against, and that being (W.a) from Table I, without causing any cross-channel interferences in the experiments. PARSAX operates in S-band with an  $f_c$  of 3.315 GHz, has an IF of 125 MHz and a  $B_T$  of 40 MHz. A block diagram of the experimental setup is presented in Fig. 7. The receiver channels were calibrated in amplitude and phase. The FPGA receiver cards (R-1) and (R-2) sample the transmitted and received signals in IF after down-conversion. The cards are from Innovative Integration model X5-400M, with Virtex-5 FPGAs and equipped with two 14-bit

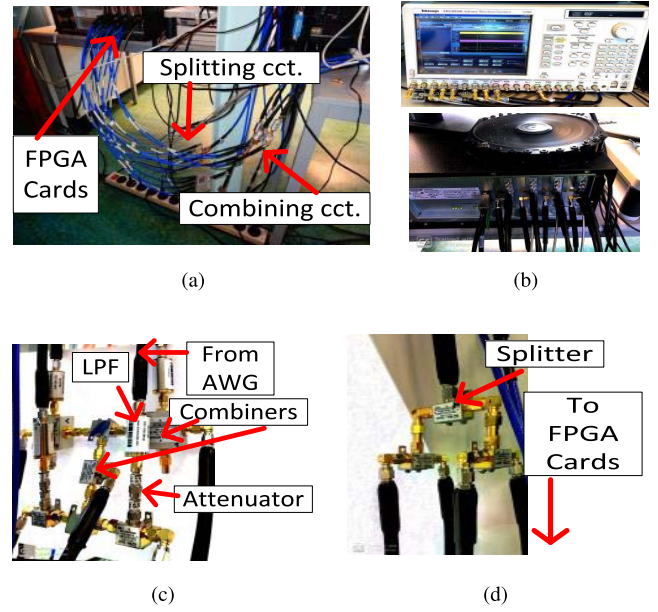


Fig. 8. Photographs of the experimental setup shown in Fig. 7 with the PARSAX radar. In (a), the connections to and from the FPGA cards are shown. In (b), the AWG – where the waveforms and triggers are setup to match what is shown at the top of Fig. 7 – and the FPGA cards on the PCIe backplane are shown. The combining and splitting circuits are shown in (c) and (d) respectively.

400 MSPs ADCs. An SSB I/Q deramping receiver architecture is implemented on the FPGAs with a 2 MHz LPF cutoff, and beat-frequency signals are transferred to a PC via PCIe interfaces connected to a PCIe-expansion backplane. Waveform (W.a) is created on the AWG Ch1. A waveform resembling (W.c) is created on Ch1, but with an alternating high and low parts, as seen in Fig. 7. Waveforms from Ch1 and Ch2 are combined in analog and sent to the transmitter circuit. A similar splitting operation is performed by an analog splitting circuit on reception. A depiction of the resultant combined waveforms is also presented in Fig. 7, where waveform (W.c) is realized using only the lower parts of the combined waveform (see horizontal shading in the figure), by extracting beat-frequency signals from both receiver boards on the PC in an alternating manner. Note that the starting phase is set to be the same for the waveform in Ch1 and the lower part of the waveform in Ch2. This allows Doppler processing on the lower part of the combined waveforms, and thus realizing waveform (W.c). Waveform (W.d) is realized as shown by the vertical shaded area, where data is extracted from alternating receivers as well. Note the triggering at 500 Hz and 1 kHz for R-1 and R2 respectively, as shown in the figure. A photograph of the experiment setup is shown in Fig. 8(a). The Arbitrary Waveform Generator (AWG) and the FPGA cards are shown in Fig. 8(b). The IF combining and splitting circuits are shown in Fig. 8(c) and Fig. 8(d) respectively. The SNR for all the experiments was around 70 dB.

### C. Experiments Description

- **Experiment-1: A Stable Target:** The industrial chimney shown in the bottom left corner of Fig. 6 is selected as a

stable target in this experiment. Its height allows the radar beam to be pointed to its top part, while avoiding most of the ground clutter. A measurement was taken before and after channels calibration to observe the effect discussed in Section IV-A.

- **Experiment-2: A Moving Targets:** A car on a traffic-quiet road on campus was selected as a moving target. A camera mounted on the radar captured its image synchronously with the radar transmission - as shown at the bottom center of Fig. 6. The car was driving at a velocity of around 12.5 m/s (45 km/h) away from the radar. The car will be ambiguous for a 500 Hz PRF, but will be unambiguous at a PRF of 1 kHz.
- **Experiment-3: An Extended-Moving Target:** A rain and clouds formation is selected as an extended-moving target. The weather formation at the moment of experiment is shown in the bottom right corner of Fig. 6, where a rain-fall rate of between 0.1 mm/h to 3 mm/h (from the color-code) is reported over Delft.

#### D. Experiments Results and Discussion

1) **Experiment-1 Results:** The results of the first experiment are presented in Fig.9.

Waveform (W.a) – as a reference – is shown in Fig.9(a), and (W.c) – before channels-calibration – in Fig.9(b) where ghost targets appear due to the phenomenon discussed in Section IV-A. Post channels-calibration, results for (W.c) are shown in Fig.9(c), where the ghost targets are still visible, but strongly suppressed, and an unambiguous Doppler-velocity interval extension from 11.3 m/s to 22.6 m/s is observed. An apparent response function width degradation is noted for the chimney (at a range around 1200 m) for (W.c) can be seen in Fig.9(c), compared to (W.a) in Fig.9(a), and its close restoration via waveform (W.d) in Fig.9(d) in comparison to (W.a). A range cut across zero-Doppler for the ranges around the chimney is presented in Fig.9(e) where (W.d) closely restores the response function width compared to (W.a), but with a higher peak to sidelobe level due to method errors and imperfections as discussed in Section IV-D. Following the approach in [20], to relate the results to a detection scenario – regardless of probability of detection and false alarm – three parameters are measured. The difference in signal amplitude (loss compared to (W.a)) for the target peak is represented by difference peak-to-peak (dP2P), the difference in peak-to-sidelobe level is represented by (dPSL), and the target response function width at the  $-3$  dB line is represented by (TRW). These parameters are presented in Table III, and a depiction of their definition is shown in Fig.9(e). (W.d) compared to (W.a) suffers a 1 dB loss for dP2P, and is 3 dB worst for dPSL due to concatenation errors as discussed in Section IV-D. As expected, (W.d) however improved the TRW from 11 m for (W.c) to 7 m.

2) **Experiment-2 Results:** Similar findings can be inferred about the results for experiment-2 as presented in Fig. 10.

The car is ambiguous at a velocity of around 10.5 m/s via (W.a) in Fig. 10(a), but its velocity is unambiguously estimated via (W.c) and (W.d) in Fig. 10(b) and Fig. 10(c)

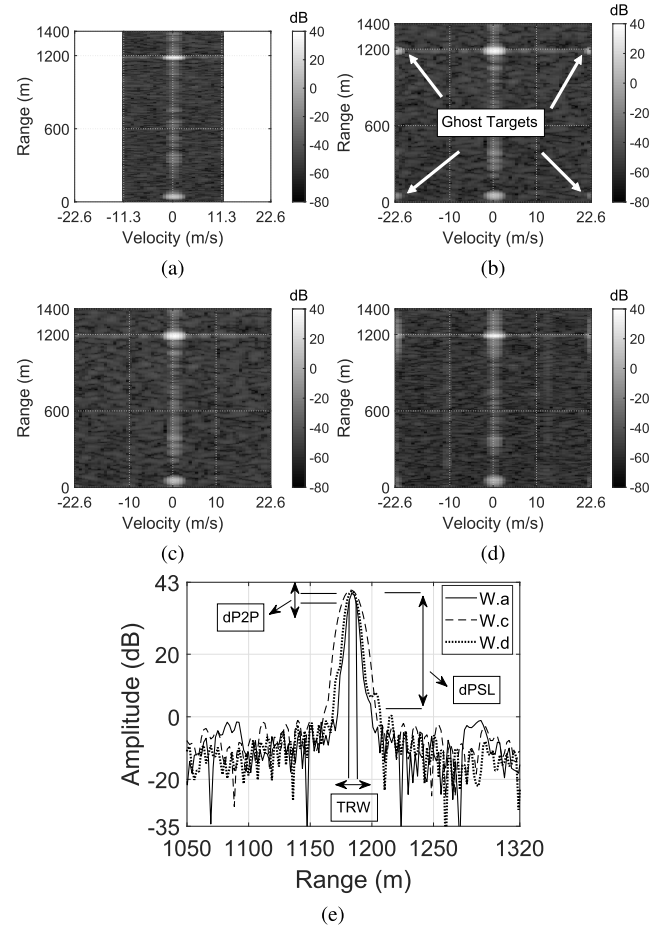


Fig. 9. Range-Velocity maps presenting results for the chimney stable-target (experiment 1) described in Section V-C. The result for waveform (W.a) – as described in Table I – is shown in (a), for waveform (W.c) before and after channels-calibration in (b) and (c) respectively, and for waveform (W.d) in (d). What appears to be ghost targets at the edges of (d) are processing artifacts due to the method's imperfections and concatenation errors, as discussed in Section IV-D. A range cut through zero-Doppler around the chimney is shown in (e), where the response function width closely matches that of (W.a), but with the Doppler ambiguity interval extension. The dP2P, dPSL and TRW parameters related to Table III are symbolically depicted in (e) to visualize their meaning.

TABLE III

RESULTS RELATED TO THE TARGET RANGE CUTS FOR THE FIRST AND SECOND EXPERIMENTS (FIG.9(E) AND FIG. 10(D)). THE DIFFERENCE IN SIGNAL AMPLITUDE (LOSS) FOR THE TARGET PEAK COMPARED TO THE REFERENCE WAVEFORM IS REPRESENTED BY DP2P.

FOR ALL WAVEFORMS, THE PEAK TO SIDELobe IS REPRESENTED BY DPSL AND THE TARGET RESPONSE FUNCTION WIDTH IS REPRESENTED BY TRW

	dP2P (dB)		dPSL (dB)		TRW (m)	
Experiment Number	1	2	1	2	1	2
(W.a)	n/a	n/a	42	32	5	9
(W.c)	.7	.2	42	32	11	20
(W.d)	1	2.5	39	31	7	11

respectively – due to the PRF increase. The car's response function width for (W.d) is improved compared to (W.c), and a range cut through the car's Doppler-velocity bin is presented in Fig. 10(d). The demonstrated improvement for (W.d) is less



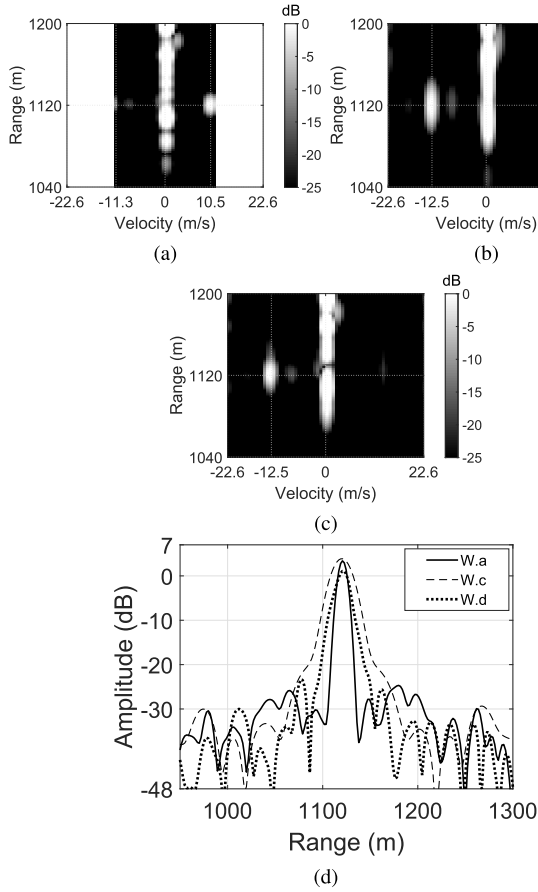


**Fig. 10.** Range-Velocity maps presenting results for the car moving-target (experiment 2) described in Section V-C. The result for waveform (W.a) – as described in Table I – is shown in (a), where the car is ambiguous at 10.5 m/s, but after the PRF increase for waveform (W.c) (W.d) shown in (b) and (c) respectively, the car's velocity is unambiguously estimated at  $-12.5$  m/s receding from the radar. A response function width improvement can be observed in (c) compared to (a), as can also be seen in range cut through car's Doppler bin. The demonstrated improvement for (W.d) is less than the theoretical expectation of it to match the performance of (W.a) is due to concatenation errors as discussed in Section IV-D.

than the theoretical expectation of it to match the performance of (W.a), which is due to concatenation errors. The parameters in Table III show that (W.d) compared to (W.a) suffers a 2.5 dB loss for dP2P, and is 1 dB worst in dPSL. As expected, (W.d) however improved the TRW from 20 m for (W.c) to 11 m.

**3) Experiment-3 Results:** The results for the weather formation of experiment-3 are presented in Fig. 11. The range-velocity matrix's zero-Doppler is clipped for all ranges, and it is then thresholded at  $-40$  dB from its strongest peak. A weighted mean Doppler velocity is then calculated for each range in the range-velocity matrix as:

$$\bar{v} = \frac{\sum_{i=-V_{\min}}^{V_{\max}} i v_i}{\sum_{i=-V_{\min}}^{V_{\max}} v_i} \quad (24)$$

where  $V_{\min}$  and  $V_{\max}$  are the minimum and maximum velocities in the unambiguous velocity interval respectively, and  $v$

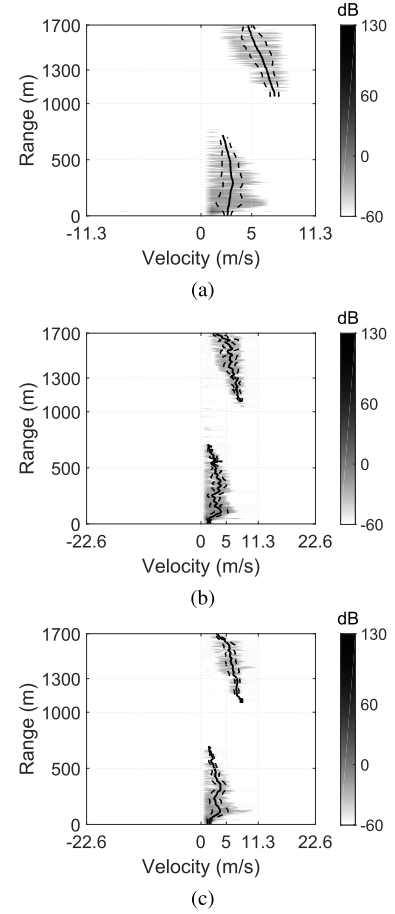


**Fig. 11.** Range-Velocity maps presenting results for the extended moving target (experiment 3) described in Section V-C. The mean velocity is presented by the solid line, and the Doppler width (positive and negative) with the dashed lines. The result for waveform (W.a) is shown in (a), where the weather formation is unambiguous and has a positive velocity as expected for rain-fall. The formation's shape is maintained for waveforms (W.c) and (W.d) as seen in (b) and (c) respectively.

is the Doppler power spectrum. A Doppler width is similarly calculated for each range as:

$$\sigma = \sqrt{\frac{\sum_{i=-V_{\min}}^{V_{\max}} (i - \bar{v})^2 v_i}{\sum_{i=-V_{\min}}^{V_{\max}} v_i}} \quad (25)$$

where  $\bar{v}$  is the average velocity for that range following (24). The mean velocity and Doppler width are also presented in Fig. 11.

An average error percentage is used to quantitatively compare the mean velocity and Doppler width for the different waveforms. This error is defined as:

$$\text{error} = \frac{1}{R} \sum_{r=1}^R \left| \frac{x_r - \hat{x}_r}{x_r} \right| \times 100\% \quad (26)$$

where  $R$  is the number of ranges tested for,  $x_r$  is the mean velocity or the Doppler width for (W.a) as a reference, and  $\hat{x}_r$  is the mean velocity or Doppler width for the waveforms compared against. The mean velocity errors for (W.c) and

(W.d) are 11.9% and 12.3% respectively. The Doppler width errors for (W.c) and (W.d) are 28.8% and 18.2% respectively. Errors related to (W.c) are due to resolution loss, and errors for (W.d) are due to the method's imperfections and concatenation errors creating sidelobes around the 5 m/s velocity point, as seen in Fig. 11(c).

The rain and clouds' shape and velocity-spread are maintained when extending the PRF for waveforms (W.c) and (W.d) as seen in Fig. 11(b) and Fig. 11(c), compared to (W.a) in Fig. 11(a).

## VI. CONCLUSION

In this paper we proposed a novel waveform and a processing method to decouple the Doppler ambiguity interval from the maximum operational range, range resolution, and processing gain in frequency multiplexed FMCW Radar. The method allowed the keeping of the radar's operational parameters while increasing the PRF – to unambiguously observe fast(er) moving targets, without having to trade-off these operational parameters. The solution proposed was to exploit the fact that beat-frequency signals have the same baseband frequencies, even if the transmitted and received chirps occupied different RF bands, with discussed limitations. That is in the sense that these baseband signals can be concatenated in the time-frequency domain to restore any operational parameters' losses due to the PRF increase. The price to be paid is to use more receiver channels in the radar. We have presented the method's limitations and an implementation feasibility analysis, where we discussed the maximum possible number of chirps to be multiplexed, and the maximum chirps' center-frequency difference. The method is verified by simulations and experiments with an FMCW radar for stable, moving and extended-moving targets. We found that the proposed method indeed alleviates the trade-off between FMCW operational parameters, and have highlighted its non-idealities in the experiments.

## ACKNOWLEDGMENT

The authors would like to thank Asst. Prof. F. Uysal for the numerous radar and signal processing discussions.

## REFERENCES

- [1] D. E. Barrick, "FMCW radar signals and digital processing," Environ. Res. Laboratories (U.S.), Washington, DC, USA, NOAA Tech. Rep. ERL 283-WPL 26, 1973.
- [2] A. Stove, "Linear FMCW radar techniques," *IEE Proc. F Radar Signal Process.*, vol. 139, no. 5, p. 343, 1992.
- [3] A. Asensio Lopez *et al.*, "Coherent signal processing for traffic flow measuring radar sensor," *IEEE Sensors J.*, vol. 18, no. 12, pp. 4803–4813, Jun. 2018.
- [4] S. Kim and K.-K. Lee, "Low-complexity joint extrapolation-MUSIC-based 2-D parameter estimator for vital FMCW radar," *IEEE Sensors J.*, vol. 19, no. 6, pp. 2205–2216, Mar. 2019.
- [5] Y. Li and S. O'Young, "Method of doubling range resolution without increasing bandwidth in FMCW radar," *Electron. Lett.*, vol. 51, no. 12, pp. 933–935, Jun. 2015.
- [6] H. L. Van Trees, *Optimum Array Processing: Part IV of Detection, Estimation, and Modulation Theory*. Hoboken, NJ, USA: Wiley, 2002.
- [7] N. Levanon, E. Mozeson, and C. Levanon, *Radar Signals*. Hoboken, NJ, USA: Wiley, 2004.

- [8] J. Yu and J. Krolik, "Multiband chirp synthesis for frequency-hopped FMCW radar," in *Proc. Conf. Rec. 43rd Asilomar Conf. Signals, Syst. Comput.*, 2009, pp. 1315–1319.
- [9] V. K. Nguyen and M. D. Turley, "Bandwidth extrapolation of LFM signals for narrowband radar systems," in *Proc. Int. Conf. Radar*, Sep. 2013, pp. 140–145.
- [10] M. Pan, B. Chen, and M. Yang, "A general range-velocity processing scheme for discontinuous spectrum FMCW signal in HFSWR applications," *Int. J. Antennas Propag.*, vol. 2016, pp. 1–13, 2016.
- [11] A. Lulu and B. G. Mobasser, "Phase matching of coincident pulses for range-Doppler estimation of multiple targets," *IEEE Signal Process. Lett.*, vol. 26, no. 1, pp. 199–203, Jan. 2019.
- [12] K. B. Cooper, S. L. Durden, C. J. Cochrane, R. R. Monje, R. J. Dengler, and C. Baldi, "Using FMCW Doppler radar to detect targets up to the maximum unambiguous range," *IEEE Geosci. Remote Sens. Lett.*, vol. 14, no. 3, pp. 339–343, Mar. 2017.
- [13] K. Armanious, S. Abdulatif, F. Aziz, U. Schneider, and B. Yang, "An adversarial super-resolution remedy for radar design trade-offs," in *Proc. 27th Eur. Signal Process. Conf. (EUSIPCO)*, A Coruña, Spain, Sep. 2019, pp. 1–5.
- [14] M. Jankiraman, *Design of Multi-Frequency CW Radars*. Rijeka, Croatia: SciTech, 2007.
- [15] G. Babur, "Processing of dual orthogonal CW polarimetric radar signals," Ph.D. dissertation, TU Delft, Delft, The Netherlands, 2009.
- [16] W. L. Melvin and J. A. Scheer, *Principles of Modern Radar: Radar Applications*, vol. 3. Rijeka, Croatia: SciTech, 2014.
- [17] S. Neemat, F. Uysal, O. Krasnov, and A. Yarovoy, "Reconfigurable range-Doppler processing and range resolution improvement for FMCW radar," *IEEE Sensors J.*, vol. 19, no. 20, pp. 9294–9303, Oct. 2019.
- [18] M. A. Richards, *Fundamentals of Radar Signal Processing*. New York, NY, USA: McGraw-Hill, 2014.
- [19] G. M. Brooker, "Understanding millimetre wave FMCW radars," in *Proc. 1st Int. Conf. Sens. Technol.*, Palmerston North, New Zealand, 2005, pp. 152–157.
- [20] S. Neemat, O. Krasnov, and A. Yarovoy, "An interference mitigation technique for FMCW radar using beat-frequencies interpolation in the STFT domain," *IEEE Trans. Microw. Theory Techn.*, vol. 67, no. 3, pp. 1207–1220, Mar. 2019.
- [21] O. A. Krasnov, L. P. Ligthart, Z. Li, G. Babur, Z. Wang, and F. van der Zwan, "PARSAX: High-resolution Doppler-polarimetric FMCW radar with dual-orthogonal signals," in *Proc. 18th Int. Conf. Microw. Radar Wireless Commun. (MIKON)*, 2010, pp. 1–5.



**Sharef Neemat** received the B.S. degree in computer engineering from King Saud University (KSU) in 2004 and the M.Sc. degree in electrical engineering from the University of Cape Town (UCT) in 2010. He is currently pursuing the Ph.D. degree with the Faculty of Electrical Engineering, Mathematics, and Computer Science (EEMCS), Microwave Sensing, Signals and Systems (MS3) Section, Delft University of Technology, Delft, The Netherlands. His study focused on secondary surveillance radar (SSR) identification friend or foe (IFF). Before and after receiving his M.Sc., he was involved in airborne radios work in the form of design, development, and test of field programmable gate array (FPGA)/digital signal processor (DSP) drivers and application layer SW for radio housekeeping and scheduling. The DSP designs and code were developed to comply with DO-178B level C (Software Considerations in Airborne Systems and Equipment Certification) and Motor Industry Software Reliability Association (MISRA) C standard. He was furthermore responsible for system engineering/project management of asset-tracking-systems' development. The work had involved writing system engineering management plans and requirements documentation for systems and their sub-systems, complying with MIL-STD-490 and MIL-STD-491.



**Oleg Krasnov** received the M.S. degree in radio physics from Voronezh State University, Russia in 1982, and the Ph.D. degree in radiotechnique from the National Aerospace University "Kharkov Aviation Institute," Ukraine, in 1994. In 1999, he joined the International Research Center for Telecommunications and Radar (IRCTR), TU Delft. Since 2009, he has been a Senior Researcher with the Faculty of Electrical Engineering, Mathematics, and Computer Science (EEMCS), Microwave Sensing, Signals and Systems (MS3) Section, Delft University of Technology, where he became a Universitair Docent (an Assistant Professor) in 2012. His research interests include radar waveforms, signal and data processing algorithms for polarimetric radars and distributed radar systems, multisensor atmospheric remote sensing, optimal resource management of adaptive radar sensors, and distributed systems. He has served as the Secretary of the 9th European Radar Conference (EuRAD'12), Amsterdam, The Netherlands.



**Fred van der Zwan** was born in The Hague, The Netherlands. He received Diploma degree from the Electronic Technical School, The Hague, in 1986.

After working at institutes like Toshiba, TNO, and TU Delft, in 1992, he became an Electronic Designer with the Telecommunications and Tele-Observation Technology Group. He initiated and coordinated several new radar projects and campaigns. He had many contacts with all participating partners in several projects. In January 2004, he became a Co-Applicant of the PARSAX Project which was granted in December 2005. After that, he became a Technical Coordinator of the PARSAX Project. In 2010, he became a Technical Coordinator with the Radar Department. In 2017, he became a Drone Pilot. He wrote an operational manual and received a certificate to perform drone flights for research purposes for TU Delft. He is currently with the Faculty of Electrical Engineering, Mathematics, and Computer Science (EEMCS), Microwave Sensing, Signals and Systems (MS3) Section, Delft University of Technology, Delft, The Netherlands.



**Alexander Yarovoy** (Fellow, IEEE) received the Diploma (Hons.) degree in radiophysics and electronics, and the Cand. Phys. and Math. Sci. in radiophysics and the Dr. Phys. and Math. Sci. degree in radiophysics from Kharkov State University, Kharkov, Ukraine, in 1984, 1987, and 1994, respectively. In 1987, he joined the Department of Radiophysics, Kharkov State University, as a Researcher, where he became a Professor in 1997. From 1994 to 1996, he was with the Technical University of Ilmenau, Ilmenau, Germany, as a Visiting Researcher. Since 1999, he has been with the Delft University of Technology, Delft, The Netherlands. Since 2009, he has been the Chair of Microwave Sensing, Signals, and Systems. He has authored or coauthored over 250 scientific or technical articles and 14 book chapters. He holds four patents. His current research interests include ultrawideband microwave technology and its applications (particularly radars), and applied electromagnetics (particularly UWB antennas).

Prof. Yarovoy was a corecipient of the European Microwave Week Radar Award for the article that best advances the state of the art in radar technology in 2001 (together with L. P. Ligthart and P. van Genderen) and in 2012 (together with T. Savelyev) and the Best Paper Award of the Applied Computational Electromagnetic Society in 2010 (together with D. Caratelli). He has served as a Guest Editor for five Special Issues for IEEE TRANSACTIONS and other journals. From 2011 to 2018, he has been an Associate Editor of the *International Journal of Microwave and Wireless Technologies*. He has served as the Chair and the TPC Chair for the Fifth European Radar Conference, Amsterdam, The Netherlands. From 2008 to 2017, he was the Director of the European Microwave Association.